Supporting Information

Three-Dimensionally Ordered Macroporous $La_{0.6}Sr_{0.4}MnO_3$ Supported Ag Nanoparticles for the Combustion of Methane

Hamidreza Arandiyan,[a] Hongxing Dai,*[b] Jiguang Deng,[b] Yuan Wang,[b,c] Hongyu Sun,[d] Shaohua Xie,[b] Bingyang Bai,[a] Yuxi Liu,[b] Kemeng Ji,[b] Junhua Li*,[a]

[a]*State Key Joint Laboratory of Environment Simulation and Pollution Control (SKLESPC), School of Environment, Tsinghua University, Beijing 100084, China*

[b]*Laboratory of Catalysis Chemistry and Nanoscience, Department of Chemistry and Chemical Engineering, College of Environmental and Energy Engineering, Beijing University of Technology, Beijing 100124, PR China*

[c]*National Research Center for Geoanalysis, Beijing 100037, China*

[d]*Beijing National Center for Electron Microscopy, School of Materials Science and Engineering, The State Key Laboratory of New Ceramics and Fine Processing, Key Laboratory of Advanced Materials (MOE), Tsinghua University, Beijing 100084, China.*

* Authors to whom correspondence should be addressed:

Prof. Hongxing Dai (H. X. Dai)

Tel. No.: +86-10-6739-6118; fax: +86-10-6739-1983

E-mail: hxdai@bjut.edu.cn

Prof. Junhua Li (J. Li)

Tel. No.: +86-10-6277-1093; fax: +86-10-6277-1093

E-mail: lijunhua@tsinghua.edu.cn

Content

Catalyst characterization procedures

The X-ray diffraction (XRD) experiments were performed on a Philips PW-1800 diffractometer using Cu Kα radiation (λ = 0.1.5406 nm) at 40 kV and 30 mA to determine the crystalline phases and to -calculate lattice parameters. Scattering intensities were measured over an angular range of $4^o < 2\theta < 90^o$ for all of the samples with a step size (2θ) of 0.03^o and a count time of 2 s per step. The diffraction patterns were indexed by comparison with the JCPDS (Joint Committee on Powder Diffraction Standards) files. The morphologies of the as-prepared catalysts were studied by scanning electron microscopy (SEM) using a Philips XL30 microscope operating at an accelerating voltage of 30 kV, with a work distance (WD) between 10 and 13 mm. For the determination of the chemical compositions of the crystalline phases, energy-dispersive spectroscopy (EDS) was used to determine the EDS spectra using an EDS DX-4 analysis system. A very thin Au deposit was used to improve the conductivity of the sample. Transmission electron microscopic (TEM) images as well as the selected-area electron diffraction (SAED) patterns of the typical samples were recorded on a JEOL JEM-2010 apparatus. The N_2 adsorption-desorption isotherms, surface areas, and pore parameters of the samples were determined via N_2 adsorption at −196 ^{o}C on a Micromeritics ASAP 2020 adsorption analyzer. Before measurement, the samples were degassed at 250 ^{o}C for 3 h. The surface areas and pore size distributions were calculated using the Brunauer-Emmett-Teller (BET) and Barrett-Joyner-Halenda (BJH) methods.

Hydrogen temperature-programmed reduction (H_2-TPR) studies were performed with an Autochem II 2920 (Micromeritics) apparatus equipped with a TCD detector. The experiments were conducted on the samples (approximately 50 mg). The samples were initially flushed with helium at a flow rate of 40 mL/min as the temperature was increased at a ramp rate of 10 ^{o}C/min to 200 ^{o}C and held at this temperature for 30 min to remove water.

Then, the reducing gas (5.1% H_2 in Ar) was introduced at a flow rate of 40 mL/min with a ramp rate of 10 ^oC/min from room temperature to 750 ^oC. The variation in H_2 concentration of the effluent was monitored on-line by the chemical adsorption analyzer. The reduction peak was calibrated against that of complete reduction of a known standard of powdered CuO (Aldrich, 99.995%).

Thermal analysis (TGA-DTA)

Thermal analysis of the typical samples was carried out on a TA 2960 simultaneous thermogravimetric analysis (TGA) and differential thermal analysis (DTA) apparatus. Samples (10 mg) of the samples were dried at 50 ^oC for 24 h prior to the experiments. These were then heated in air in ceramic crucibles at a rate of 2 ^oC/min from room temperature to 400 ^oC, and then at 5 ^oC/min from 400 to 750 ^oC. The thermo balance was appropriately standardized by running a thermogram on an empty crucible so as to correct for the air buoyancy effect and then cooling down to 100 ^oC (5 ^oC/min) under a flow of air at a rate of 100 mL/min. The mass loss in the temperature range was observed by TGA.

X-ray photoelectron spectroscopic (XPS)

The X-ray photoelectron spectroscopic (XPS) technique was used to determine the La 3d, Sr 2p, Mn 2p, and O 1s binding energies (BEs) of surface lanthanum, strontium, manganese, and oxygen species with Mg Kα ($h\nu$ = 1253.6 eV) as the excitation source. Before XPS measurement, the sample was treated in an O_2 flow of 20 mL/min at 200 ^oC for 1 h. After being cooled to RT, the pretreated sample was transferred to a holder in a Glove Bag (Instruments for Research and Industry, USA) that was filled with helium, and then the

holder was transferred into the spectrometer chamber under helium. The sample was outgassed (0.5 h) in the preparation chamber before being analyzed in the analysis chamber. The BE values of La 3d, Sr 2p, Mn 2p, and O 1s were calibrated against the C 1s signal (BE = 284.6 eV) of contaminant carbon.

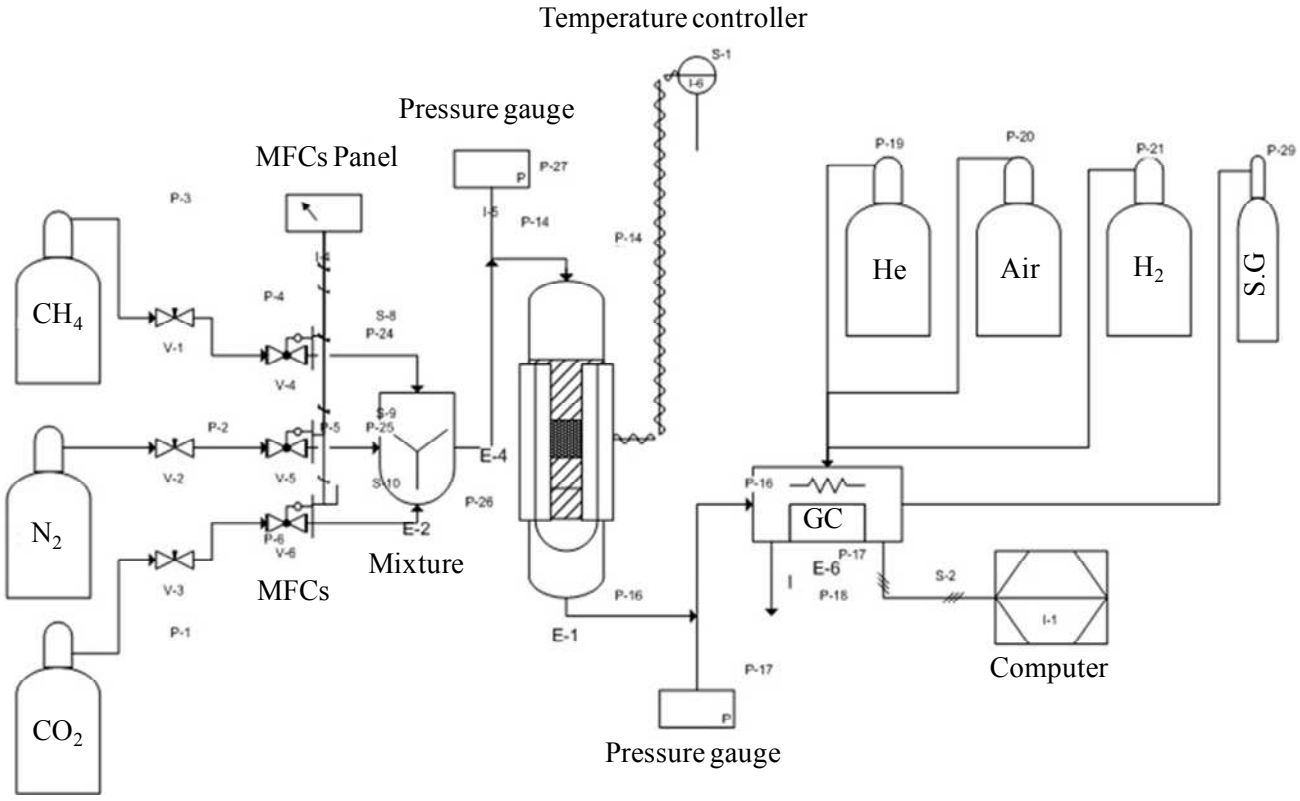

Fig. S1. Schematic diagram of the experimental set-up.

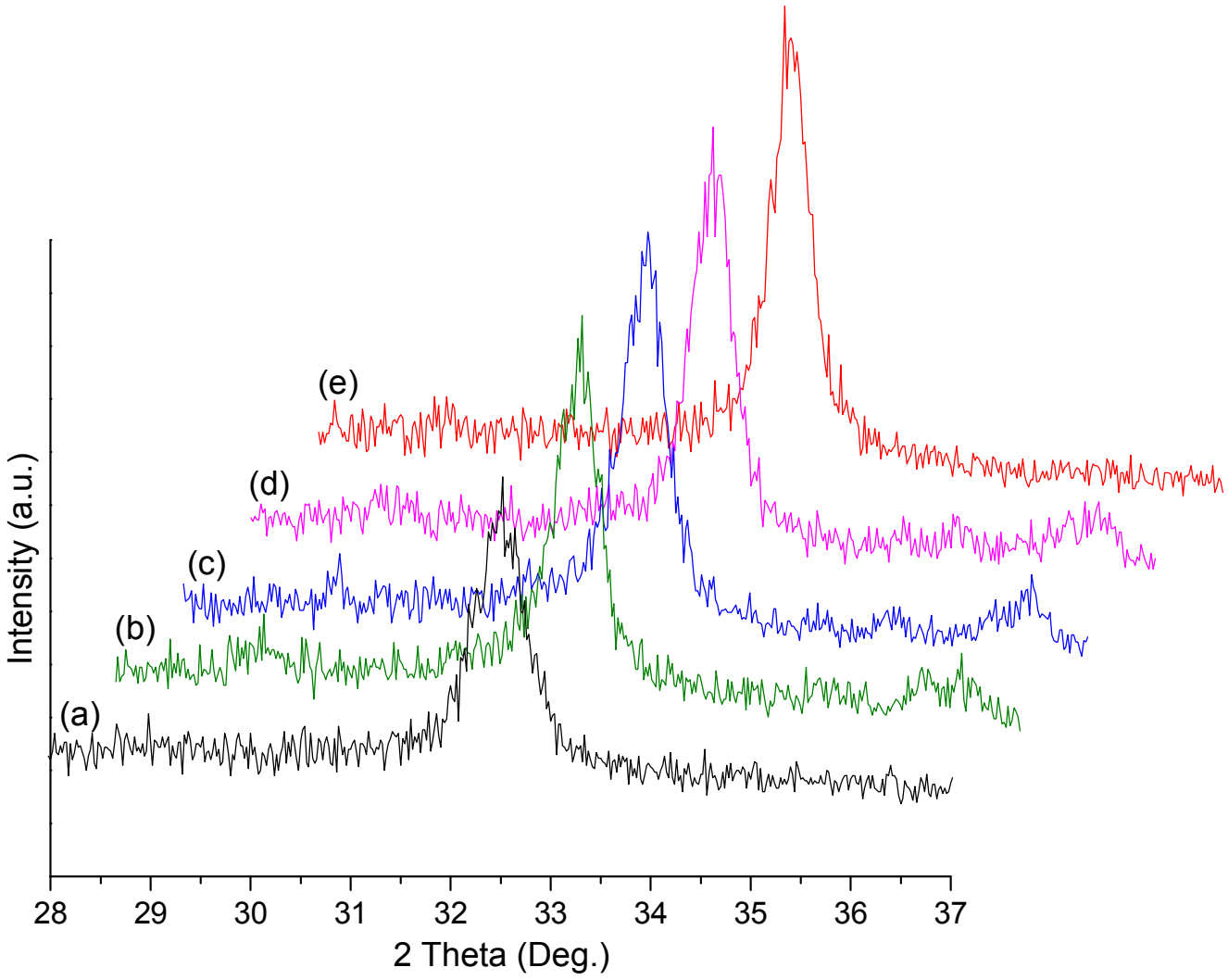

Fig. S2. Evolution of the XRD highest peak of (a) Bulk $La_{0.6}Sr_{0.4}MnO_3$, (b) 3DOM $La_{0.6}Sr_{0.4}MnO_3$, (c) l.58 wt% Ag/3DOM $La_{0.6}Sr_{0.4}MnO_3$, (d) 3.63 wt% Ag/3DOM $La_{0.6}Sr_{0.4}MnO_3$, and (e) 5.71 wt% Ag/3DOM $La_{0.6}Sr_{0.4}MnO_3$.

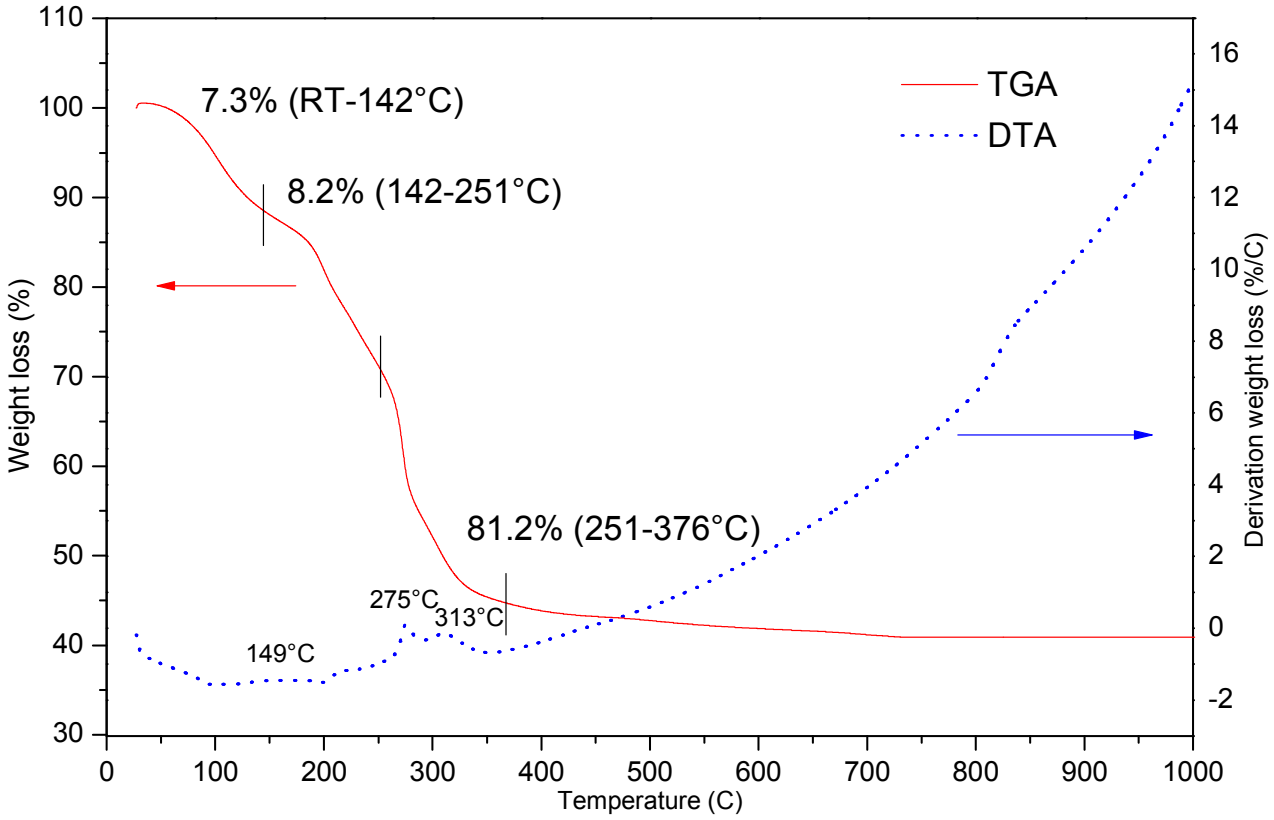

Fig. S3. TGA/DTA profiles of the 3DOM $La_{0.6}Sr_{0.4}MnO_3$ sample before calcination at 300 °C in N_2 (50 mL/min) for 3 h.

TGA/DSC results:

Fig. S3 shows the TGA/DTA profile of the uncalcined 3DOM $La_{0.6}Sr_{0.4}MnO_3$ sample. From Fig. S3, one can observe that there were weight losses of ca. 7.3, 8.2, and 81.2 wt% in the range of RT-142, 142-251, and 251-37 ^oC, respectively, accompanying by the three endothermic peaks that were assignable to the evaporation of adsorbed water, methanol, and the partial decomposition of $La(NO_3)_3$ and $Mn(NO_3)_2$ [1, 2]. The weight loss of ca. 7.3 wt% appeared in the range of RT-142 ^oC, together with the appearance of three endothermic peaks

centered at 149, 275, 313 ^{o}C, which was due to the oxidative composition of lanthanum oxide. Accompanying by the appearance of an endothermic signal at 149 ^{o}C; the second one (ca. 8.2 wt%) in the range of 142-251 ^{o}C was due to the decomposition of the remaining $La(NO_3)_3$ and $Mn(NO_3)_2$ [1], accompanying by the recording of an endothermic signal at 313 ^{o}C; and the third one (ca. 81.2 wt%) in the 251-37 ^{o}C range was attributable to the oxidative decomposition of the PMMA template [3, 4], together with the detection of an endothermic peak at 376 ^{o}C. These weight losses could be reasonably assigned to the evaporation of adsorbed water, methanol, DMOTEG and/or PEG400, and the formation of the metal-PEG complexes, the thermal decomposition of metal-PEG complexes, and the elimination of remaining PEG400, DMOTEG, and PMMA [3]. No further weight losses took place when the temperature was above 380 ^{o}C, indicating that all of the adsorbed water and organic molecules had been removed above 380 ^{o}C. In other words, the calcination conditions were appropriate for the generation of single-phase perovskite-type oxide $La_{0.6}Sr_{0.4}MnO_3$ and the complete removal of the organics employed in the preparation processes. The formation of perovskite $La_{0.6}Sr_{0.4}MnO_3$ could be further confirmed by the XRD results shown in Fig. 1.

References:

[1] Y.X. Liu, H.X. Dai, Y.C. Du, J.G. Deng, L. Zhang, Z.X. Zhao, Appl. Catal. B 119–120 (2012) 20.

[2] Y.X. Liu, H.X. Dai, Y.C. Du, J.G. Deng, L. Zhang, Z.X. Zhao, C.T. Au, J. Catal. 287 (2012) 149.

[3] H.N. Li, L. Zhang, H.X. Dai, H. He, Inorg. Chem. 48 (2009) 4421.

[4] M. Sadakane, T. Horiuchi, N. Kato, C. Takahashi, W. Ueda, Chem. Mater. 19 (2007) 5779.

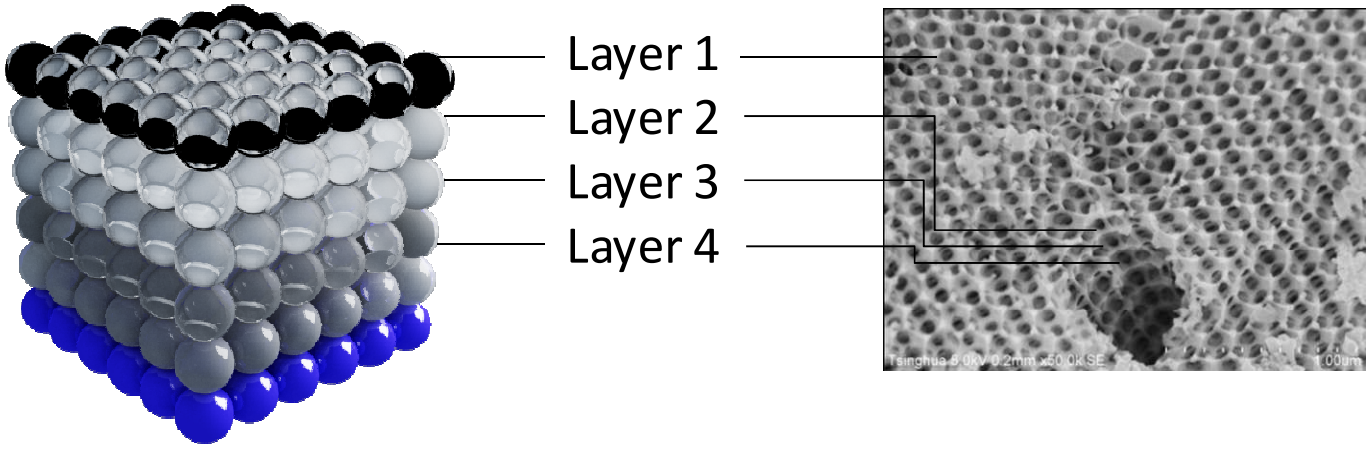

Fig. S4. Four discrete layers can be seen with interconnected through the open window within each layer.

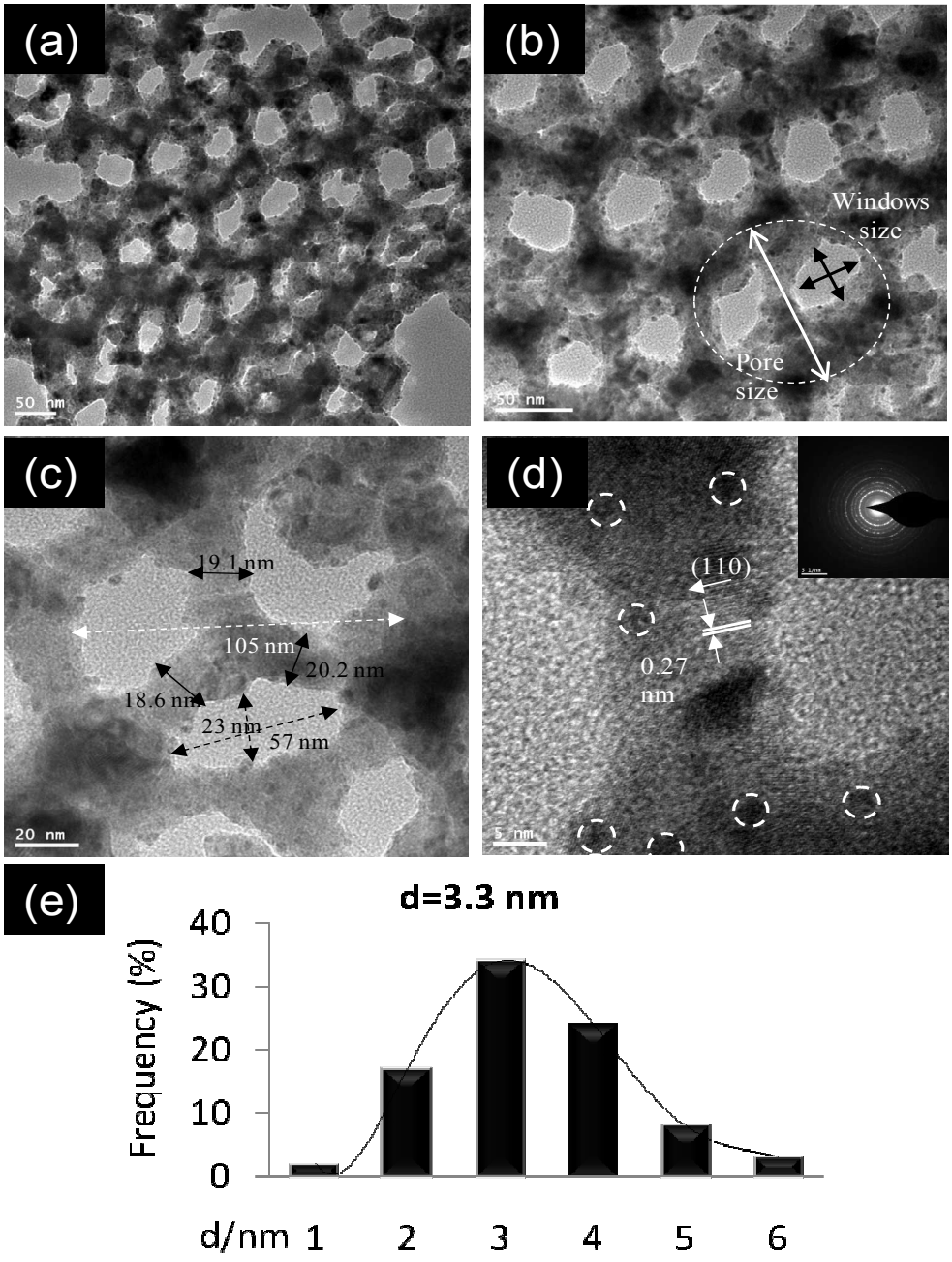

Fig. S5. TEM images (a, b) and HRTEM images (c, d) and size distribution of Ag nanoparticles (e) of 1.58 wt% Ag/3DOM $La_{0.6}Sr_{0.4}MnO_3$. The white circles of (d) clearly showing the lattice fringes of Ag suggests the formation of small Ag NPs on the 3DOM $La_{0.6}Sr_{0.4}MnO_3$ support.

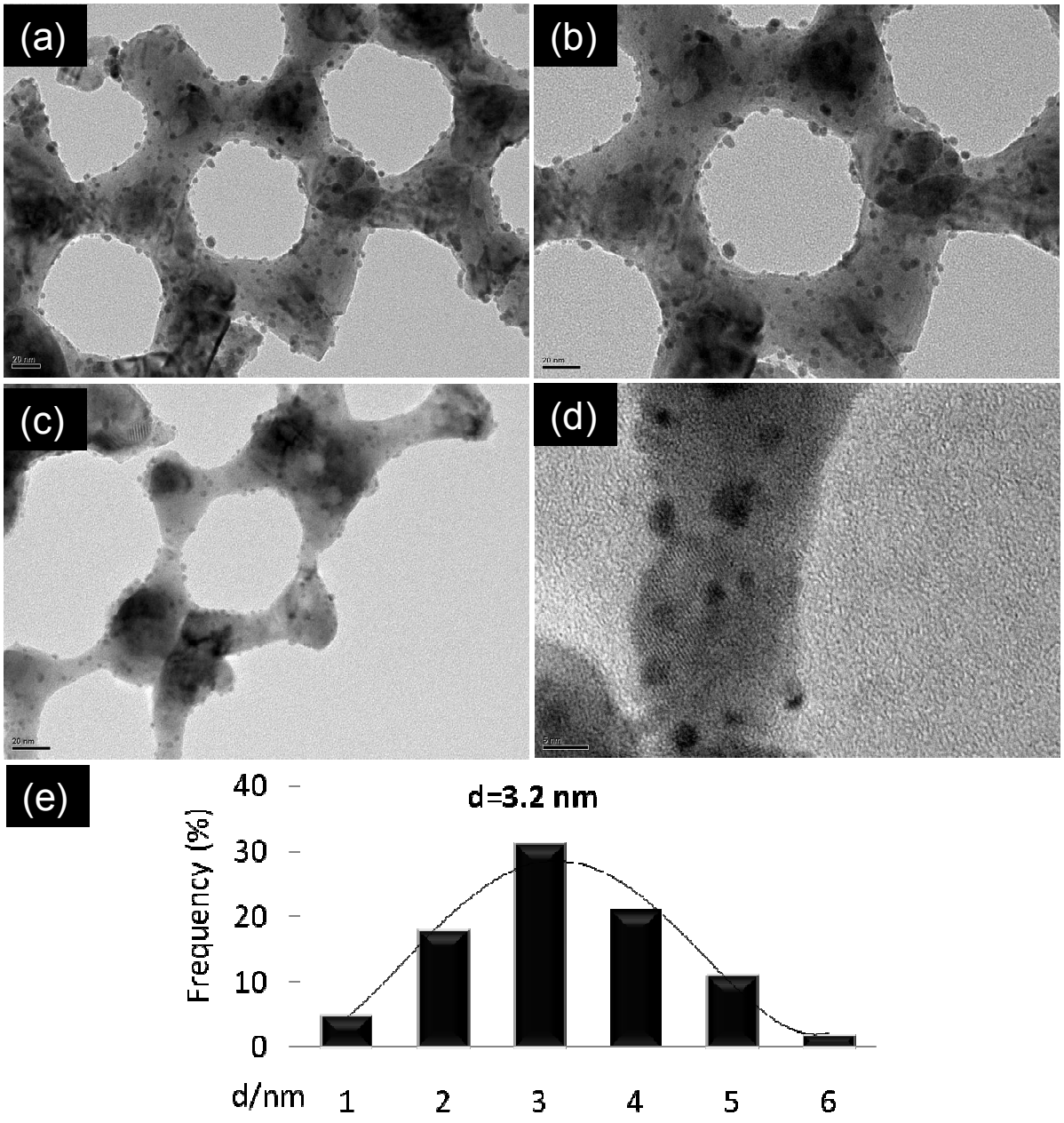

Fig. S6. TEM (a-c) and HRTEM (d) images and size distribution of Ag NPs by statistic analysis of more than 200 Ag particles in the HRTEM image (e) of 3.63 wt% Ag/3DOM $La_{0.6}Sr_{0.4}MnO_3$.

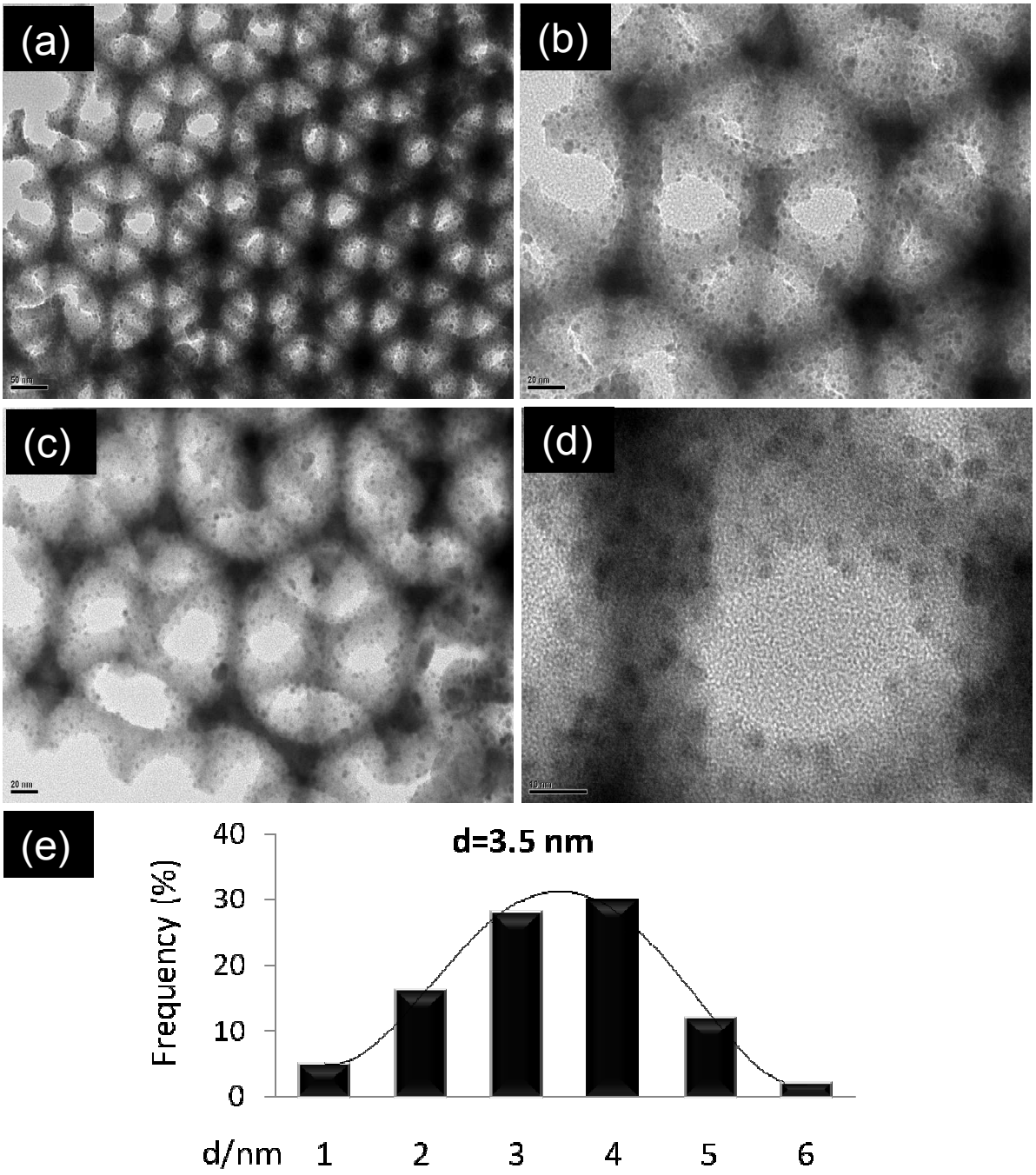

Fig. S7. TEM (a-c) and HRTEM (d) images and size distribution of Ag NPs by statistic analysis of more than 200 Ag particles in the HRTEM image (e) of 5.71 wt% Ag/3DOM $La_{0.6}Sr_{0.4}MnO_3$ catalyst.

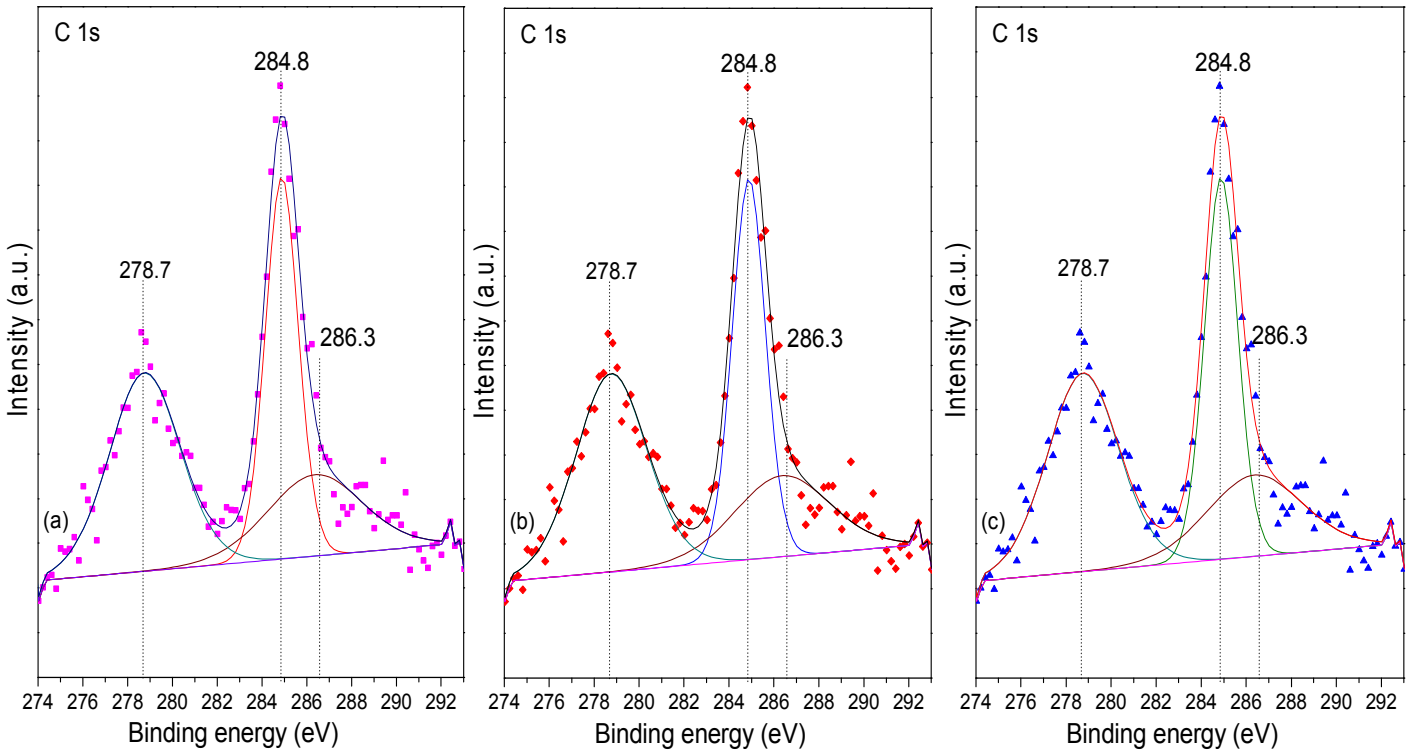

Fig. S8. C 1s XPS spectra of (a) 1.58 wt% Ag/3DOM $La_{0.6}Sr_{0.4}MnO_3$, (b) 3.63 wt% Ag/3DOM $La_{0.6}Sr_{0.4}MnO_3$, and (c) 5.71 wt% Ag/3DOM $La_{0.6}Sr_{0.4}MnO_3$.

XPS C 1s results:

Fig. S8 shows the C 1s XPS spectra of the three samples. One can clearly observe that there was a similar symmetrical C 1s XPS signal at ca. 278.7 and 284.8 eV for each sample, which generally came from the contaminated carbon. However, another rather weak C 1s signal at BE = ca. 286.3 eV appeared in each of the three samples (1.58 wt% Ag/3DOM $La_{0.6}Sr_{0.4}MnO_3$, 3.63 wt% Ag/3DOM $La_{0.6}Sr_{0.4}MnO_3$, and 5.71 wt% Ag/3DOM

$La_{0.6}Sr_{0.4}MnO_3$) which was due to the surface carbonate species [1,2]. Therefore, no significant amounts of carbonate species were formed on the surface of the three samples. Although each of the catalyst samples was pretreated in an O_2 flow of 20 mL/min at 450 ^oC for 1 h before XPS measurements, which could minimize the amounts of OH^- and carbonate species retained on the sample surfaces, the presence of carbonate species could not be completely precluded. After carefully examining the C 1s XPS spectra (Fig. S8) of these samples, we decompose each of them to three components at BE = 284.8 and 286.3 eV (due to surface contamination carbon) and 278.7 eV (due to surface carbonate species) [3].

References:

[1] H. Falcón, J. A. Barbero, J. A. Alonso, M. J. Martínez-Lope, J. L. G. Fierro, Chem. Mater. 14 (2002) 2325–2333.

[2] J.L.G. Fierro, Catal. Today 8 (1990) 153–174.

[3] Y.N. Lee, R.M. Lago, J.L.G. Fierro, V. Cortés, F. Sapiña, E. Martínez, Appl. Catal. A 207 (2001) 17–24.

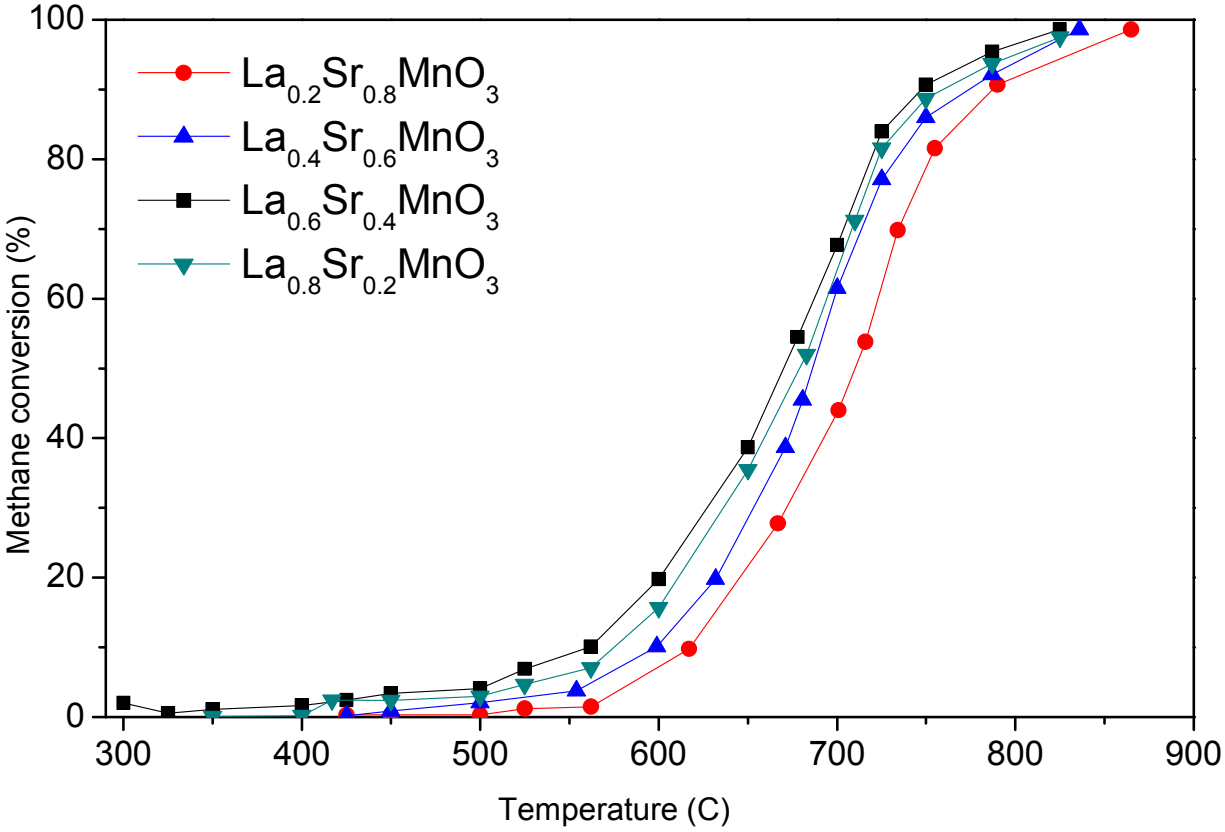

Fig. S9. Effect of Sr substitution fraction (x) on the activity of $La_{1-x}Sr_xMnO_3$ (x = 0.2, 0.4, 0.6, 0.8) catalysts for the conversion of CH_4.

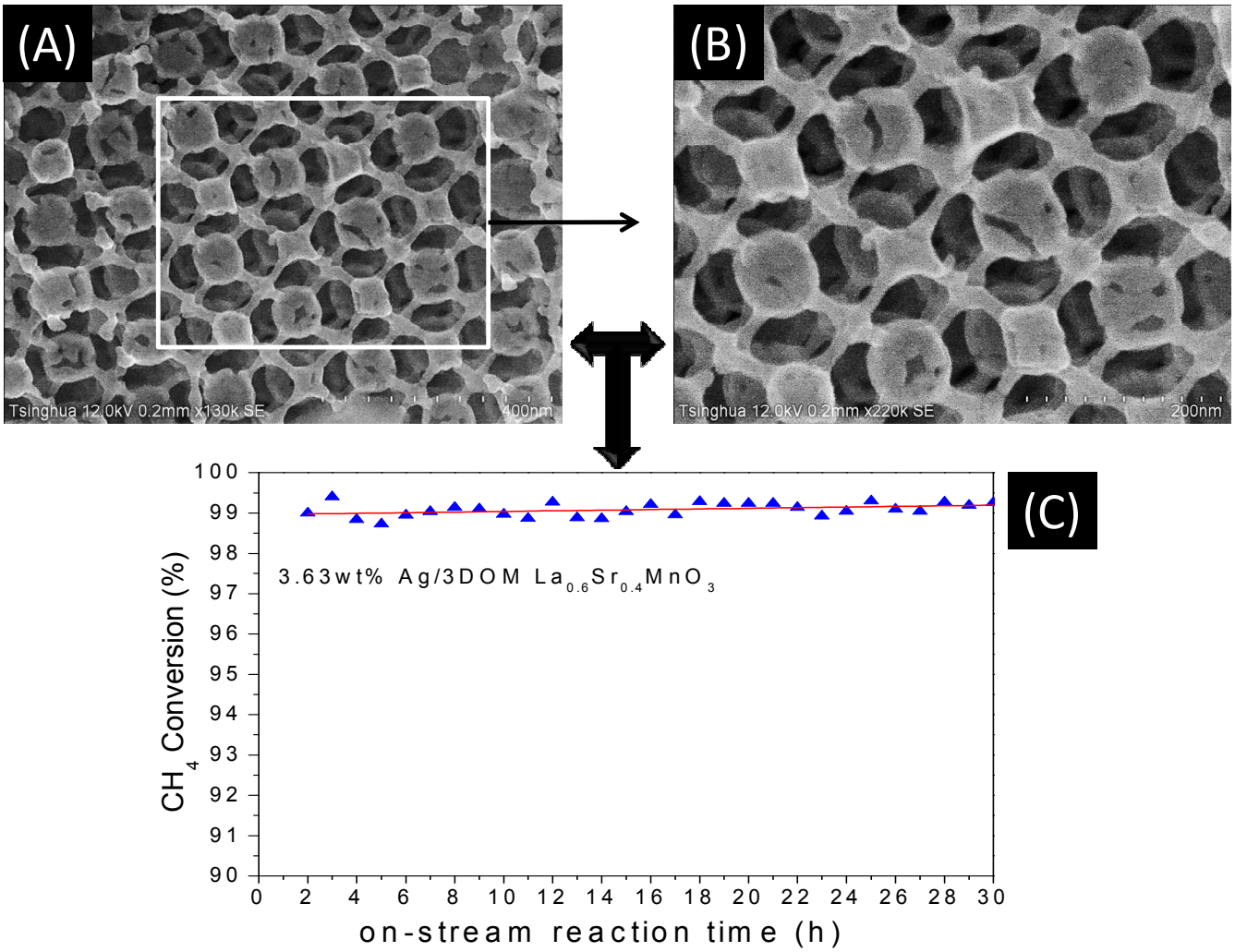

Fig. S10. SEM images (A, B) of 3.63 wt% Ag/3DOM $La_{0.6}Sr_{0.4}MnO_3$ catalyst after 30 h of on-stream reaction, and (C) CH_4 conversion versus on-stream reaction time over the 3.63 wt% Ag/3DOM $La_{0.6}Sr_{0.4}MnO_3$ at GHSV = 30,000 mL/(g h) under the conditions of 2% CH_4 + 20% O_2 + 78% N_2 (balance) and the total flow = 41.6 mL/min.

The SEM characterization results showed that the three dimensionally ordered macroporous structures were indeed formed in the as-prepared catalysts. Fig. S10 shows the SEM and HRSEM images of the 3.63 wt% Ag/3DOM $La_{0.6}Sr_{0.4}MnO_3$ catalyst after 30 h of on-stream reaction. It can be seen from the SEM images that the macrostructure of the catalyst was not remarkably changed, as compared to its fresh one.

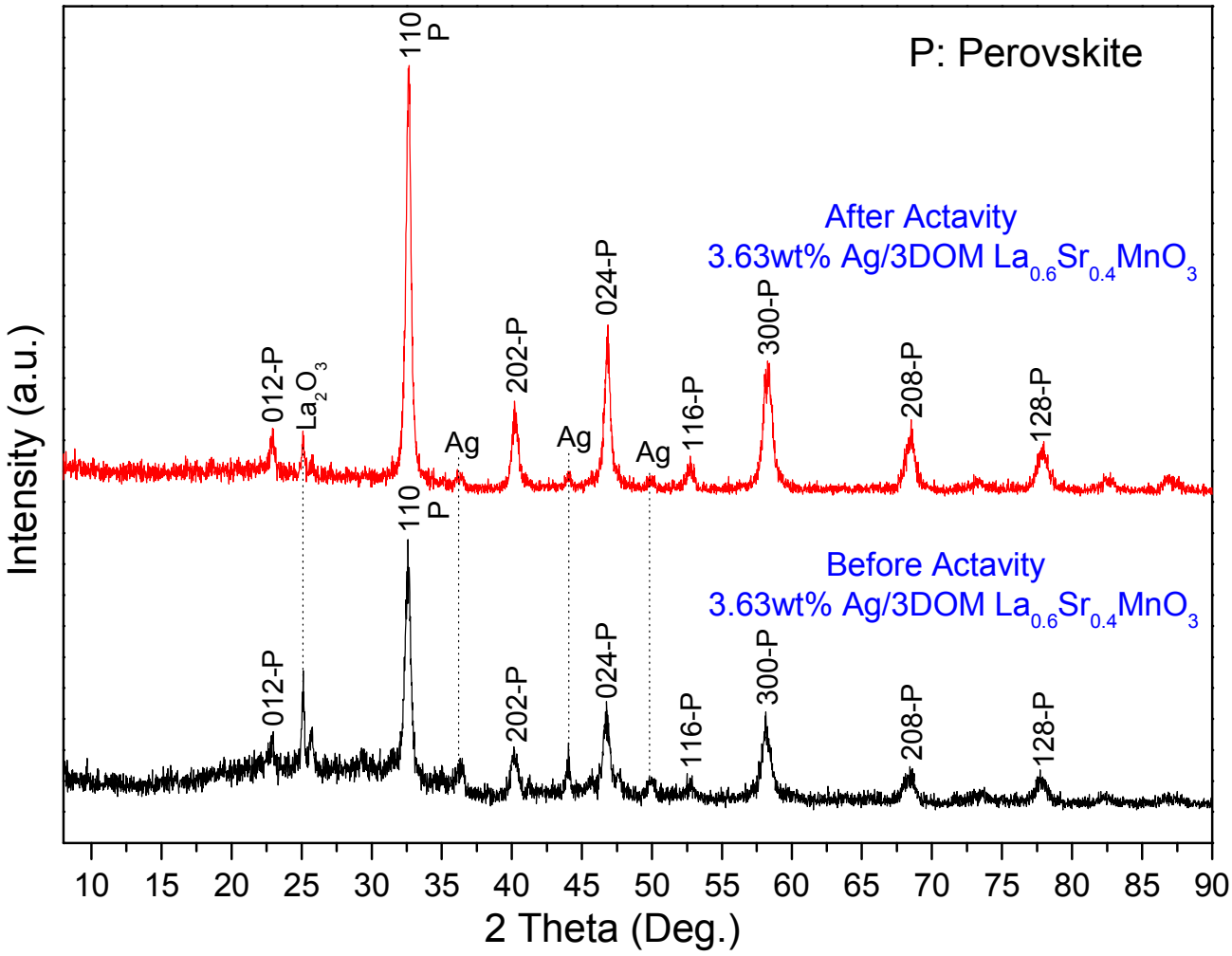

Fig. S11. XRD pattern of the 3.63 wt% Ag/3DOM $La_{0.6}Sr_{0.4}MnO_3$ sample after 20 h of on-stream reaction at GHSV = 30,000 mL/(g h) under the conditions of 2% CH_4 + 20% O_2 + 78% N_2 (balance) and the total flow = 41.6 mL/min.

To understand the structural evolution of the catalyst, we recorded the XRD pattern of the 3.63 wt% Ag/3DOM $La_{0.6}Sr_{0.4}MnO_3$ sample after 20 h of on-stream reaction. It can be observed that the used sample showed a XRD pattern rather similar to that of the fresh sample, indicating that the sample was intact after reaction.

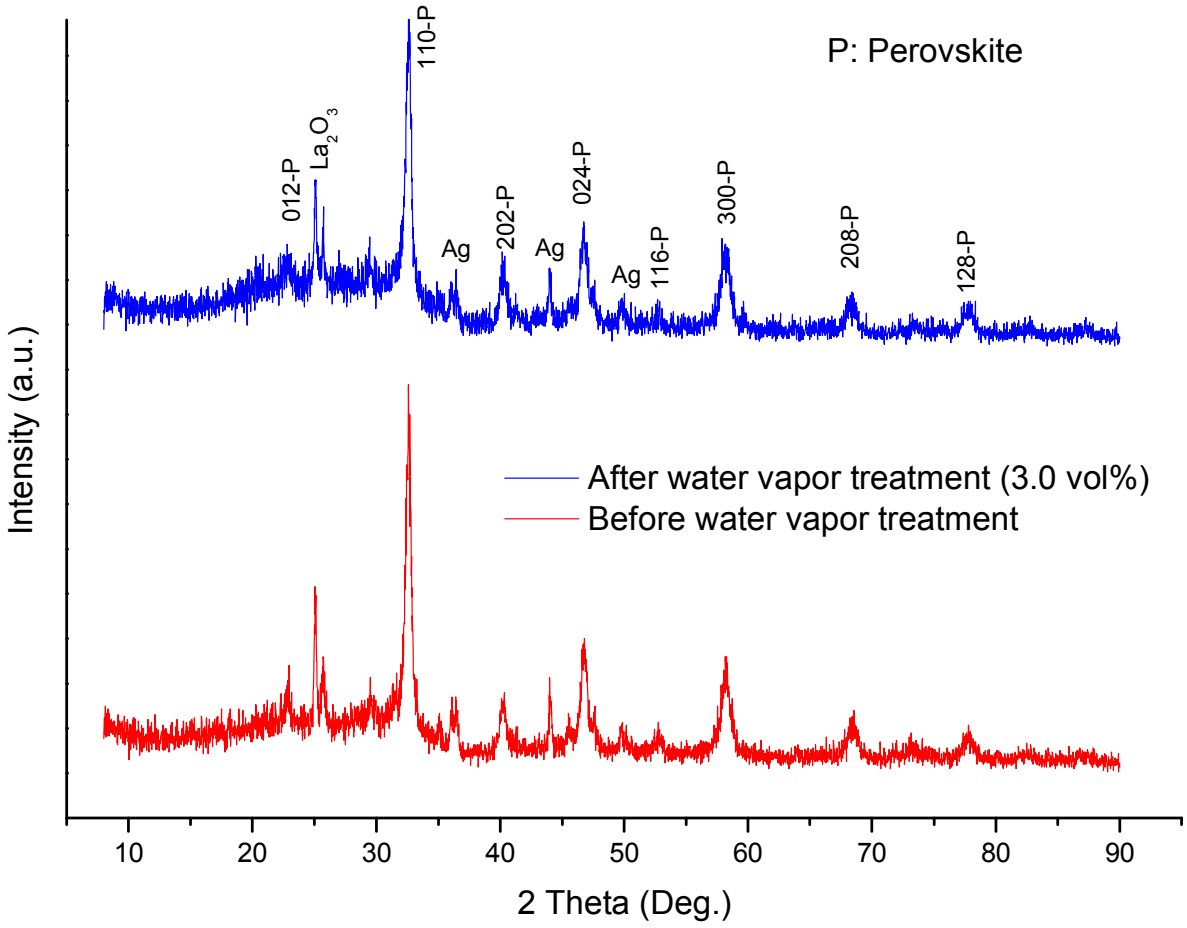

Fig. S12. XRD patterns of the fresh and used 3.63wt% Ag/3DOM $La_{0.6}Sr_{0.4}MnO_3$ sample after 10 h of on-stream reaction in the presence of 3.0 vol% H_2O under the conditions of GHSV = 30,000 mL/(g h) under the conditions of 2% CH_4 + 20% O_2 + 78% N_2 (balance) and the total flow = 41.6 mL/min.

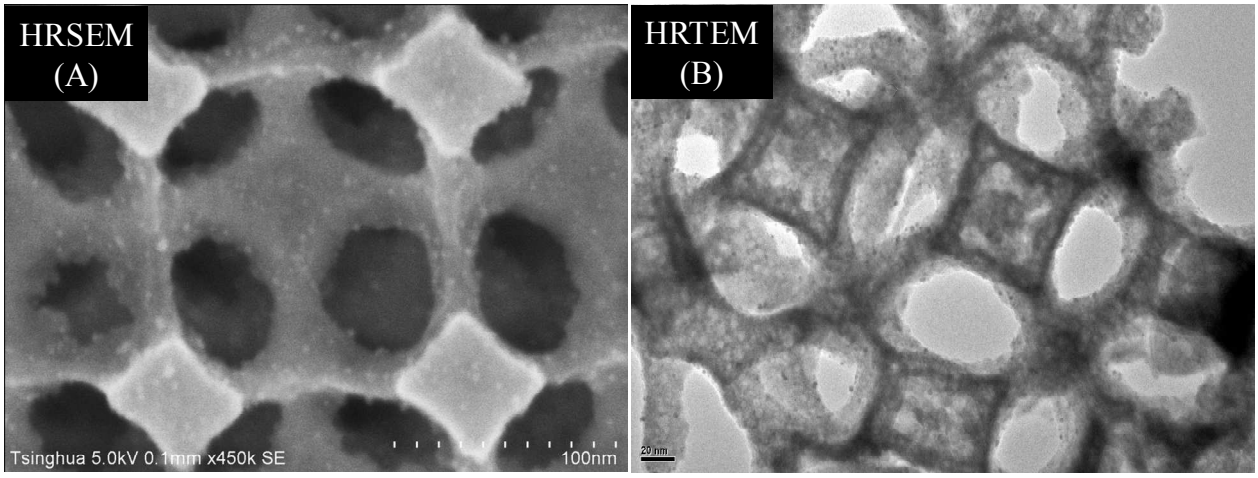

Fig. S13. (A) HRSEM and (B) HRTEM images of the used 3.63 wt% Ag/3DOM $La_{0.6}Sr_{0.4}MnO_3$ samples after 10 h of on-stream reaction in the presence of 3.0 vol% H_2O under the conditions of GHSV = 30,000 mL/(g h) under the conditions of 2% CH_4 + 20% O_2 + 78% N_2 (balance) and the total flow = 41.6 mL/min.

Table S1. Comparison of catalytic performance for the oxidation of Methane and VOCs.

Catalyst	Reactant	Concentration	Space velocity	$T_{90\%}$ (^{o}C)	Ref.
6.1 wt% Au/Fe_2O_3	Methane	1.0 vol%	51,000 h^{-1}	475 ^{o}C	7
1 wt% Pd/ZrO_2	Methane	1.0 vol%	36,000 mL/(g h)	426 ^{o}C	46
La_2CuO_4 nanorods	Methane	1.0 vol%	4,000 h^{-1}	739 ^{o}C	45
$La_{0.5}Sr_{0.5}MnO_3$	Methane	1.0 vol%	8,400 mL/(g h)	710 ^{o}C	36
20 wt% $LaMnO_3$/MgO	Methane	1.0 vol%	8,000 h^{-1}	770 ^{o}C	44
$La_{0.9}Cu_{0.1}MnO_3$	Methane	1.0 vol%	15,000 mL/(g h)	800 ^{o}C	43
6.5Au/*meso*-Co_3O_4	Methane	1.0 vol%	50,000 mL/(g h)	470 ^{o}C	56
6.5Au/*meso*-Co_3O_4	Benzene	1000 ppm	20,000 mL/(g h)	189 ^{o}C	56
6.5Au/*meso*-Co_3O_4	Toluene	1000 ppm	20,000 mL/(g h)	138 ^{o}C	56
6.5Au/*meso*-Co_3O_4	CO	1.0 vol%	60,000 mL/(g h)	–45 ^{o}C	56
4.1 wt% Au/MnO_2	Methane	1.0 vol%	51,000 h^{-1}	550 ^{o}C	7

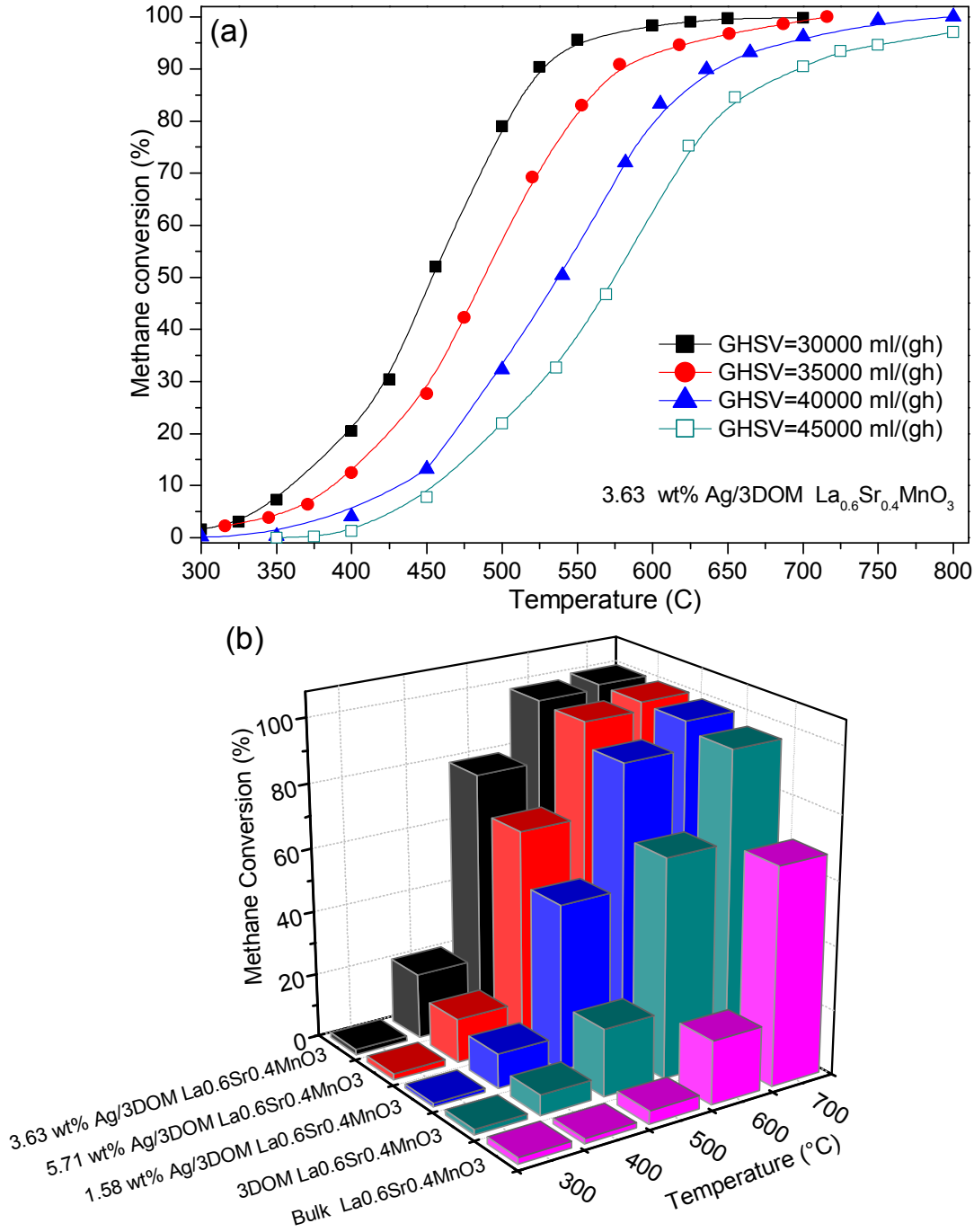

Fig. S14. (a) Effect of GHSV on the catalytic activity of the 3.63 wt% Ag/3DOM $La_{0.6}Sr_{0.4}MnO_3$ catalyst, and (b) methane conversion versus reaction temperature over the Bulk $La_{0.6}Sr_{0.4}MnO_3$, 3DOM $La_{0.6}Sr_{0.4}MnO_3$, and *y*Ag/3DOM $La_{0.6}Sr_{0.4}MnO_3$ catalysts.